Sigma J Eng Nat Sci, Vol. 42, No. 3, pp. 755–766, June, 2024

Sigma Journal of Engineering and Natural Sciences
Web page info: https://sigma.yildiz.edu.tr
DOI: 10.14744/sigma.2024.00000

Research Article

Investigation of using strain gauge in tension, torsion and bending experiments

Billur KANER[1,*], Kerem ASMAZ[1]

[1]*Faculty of Mechanical Engineering, Yildiz Technical University, 34349, İstanbul, Türkiye*

ARTICLE INFO

Article history
Received: 30 May 2022
Revised: 29 June 2022
Accepted: 23 January 2023

Keywords:
Bending; Finite Element Analysis; Strain gauge; Tension; Torsion

ABSTRACT

In the engineering approach, the calculation of stress-strain values is crucial for determining the mechanical properties of materials. It is known that stress values could be calculated using the cross-section area, the moment of inertia of the material, and even strain values. However, the experimental determination of strain values is somewhat more complicated. In strain calculation, a video- extensometer and strain gauge are generally utilized. The goal of this study is to determine the strain values of the steel material in the linear region with experimental, theoretical and numerical approaches and to examine the suitability of the use of strain gauges for bending, torsion and tensile tests. Three sets (Tension, Torsion and Bending) were prepared in the experimental approach, and strain values were obtained for each experimental set-up. Furthermore, geometric models similar to experimental design were applied to ANSYS finite element program in numerical analyses. Additionally, the strain values were determined theoretically using the full bridge approach in Wheatstone Bridge Theorem. It is thought that assessing the use of the Wheatstone bridge, examining, and comparing the theoretical approaches of different loadings, modelling the appropriate experimental methods in the finite element program, and getting results, and finally interpreting these results, make a valuable contribution to the literature. The strain values were compared. Accordingly, the mean error values between theoretical and numerical for tensile, bending and torsion tests are 5.17%, 4.23% and 6.26%, respectively. The mean error values between the theoretical-experimental results of the same tests were 7.08%, 3.48% and 4.89%, respectively. Consequently, it was seen that experimental, numerical, and theoretical approaches gave more convergence points for each test.

Cite this article as: Kaner B, Asmaz K. Investigation of using strain gauge in tension, torsion and bending experiments. Sigma J Eng Nat Sci 2024;42(3):755–766.

INTRODUCTION

Nowadays, several materials are used in many engineering practices, such as aircraft wings, turbine design, bridges and supports, and load-bearing machine elements. Materials used in engineering designs must be both durable and safe. Therefore, the mechanical properties of the material should be known to ensure that the material is

*Corresponding author.
*E-mail address: kaner@yildiz.edu.tr

This paper was recommended for publication in revised form by Regional Editor Amin Shahsavar

under durable and safe conditions. In determining the mechanical properties of materials, the usage of strain gauge takes a crucial place in literature. Non-symmetric bending deformation of Lead Zirconate Titanate (PZT) was examined using strain gauges. Theo et al. [1] stated that non-symmetric bending deformation means where the tensile strain exceed the compressive strains for a given stress level. They concluded that this phenomenon affects the mechanical behavior of PZT ceramic material. Talesnick et al. [2] stated that the applying torsional stress to hollow cylinder specimens utilizes the determination of shear modulus. In their strain calculation, the strain gauges are connected to half Wheatstone bridge configuration, and the shear strain was determined this way. Torsion tests were carried out on thin-walled tubes. In their experimental approach, four strain gauges were located on thin-walled tubes. The strain gauges measured the principal strains with an orientation of ±45° to the tube lengths. PZT ceramic material was chosen as a structural material. In addition, tensile and compression tests were applied in their experimental study. Theo et al. [3] concluded that all experimental results indicated the good agreement with the Drucker–Prager criterion. Daniel et al. [4] presented a new method for differentiating the temperature and stress effect on the resistive strain gauges made from different materials (Platinum and Titanium). Their proposed new model declared that exact determination of the gauge factors and thermal coefficients was required for strain calculations. Using strain gauges, the tensile and torsional strain was determined for the Fe48Co32P14B6 metallic glass [5]. Muhammet et al. [6] determined appropriate residual stress values in rails using strain gauges. They stated that residual stress is directly influenced the performance of rails. The studies related to the investigation of using strain gauges under different experimental conditions could be examined in the literature [7–9].

The strain gauge is used in different mechanical processes besides the determination of the mechanical behaviour of the material. Zhou et al. [10] have optimized the appropriate strain gauge placement on the structural material to improve the structures' performance. Fabio et al. [11] emphasized that experimental determination of local bone deformations due to bone implant is essential in determining the biomechanical behaviour of the bone-implant-prosthesis system. The thermal and magnetic correlation was created on the strain gauge [12]. Those strain gauges are potentially suitable for testing superconducting magnets [13].

By examining the relationship between deflection, shear force, bending and torsional moments of steel-concrete composite box girder sections for bending, shear and torsion tests for negative and positive bending, Alejandro et al. [14] found that the girder sections had a significant excess resistance concerning the shear capacity. For estimating mechanical load on circular shafts, measurements were made by placing strain gauges in different configurations and the optimum strain gauge position on the shaft was determined [15]. E. Zeinali et al. [16] investigated the torsional and lateral buckling behaviour of the beam with finite elements and by conducting experiments with strain gauges attached to fiber-reinforced polymer rods produced by the pultrusion process (PFRP) under bending stress. Experimental and numerical modelling of cold-formed C and Z-section steel beams under bending and torsional stress was compared with the predictions from the current design equation [17]. An experimental study on the quasi-static mechanical behaviour of filament-wound composite thin-walled pipes (FWC) under tensile, torsion, and multiaxial loading showed that the FWC pipe was gradually damaged in a nonlinearly until it broke under tensile load [18]. Instead of directly searching for defects in adhesively bonded single lap joints, M. Z. Sadeghi [19] used strain gauges to monitor the integrity of adhesive joints in real time.

Other studies related to different mechanical processes take place in the existing literature [20–26].

There are also studies involving determining of strain values using the Wheatstone Bridge Theorem. In designing a new combinatorial molecular device, Lafy F. Al-Badry [27] modelled it with a Wheatstone bridge consisting of four single benzene molecules and a molecular wire connected to two electrodes connecting the upper arm with the lower arm. Xin Tan et al. [28] designed and produced AlGaN/GaN pressure sensors with a Wheatstone bridge structure. W. C. Ang et al. [29] investigated the design of a Wheatstone bridge with a titanium nitride metal thin film structure as infrared (IR) sensing material and simulation to predict the performances of a resistive uncooled microbolometer. Teodor et al. [30] determined the displacement sensitivity of piezoresistive Wheatstone bridge cantilevers based on the measurement of force constant and resonance frequency for beams of various geometries by applying a scanning probe microscope. For permeability through thin-film composite (TFC) membranes, the Wheatstone bridge resistive analog model proposed by Karode et al. [31] was validated with experimental gas permeability data. Dariusz Rozumek et al. [32] conducted tests under pure bending and pure torsion and cyclic proportional, non-proportional, and random bending with torsion with the MZGS-200PL fatigue control system test stand. They analyzed the electrical signals from the existing electronic control system of the MZGS-200PL fatigue machine and the Wheatstone bridges with a strain gauge under random loading. A. Svete et al. [33] have verified the solutions of the physical-mathematical model of a potential linear flowmeter for direct mass flow measurements with the hydraulic Wheatstone measuring bridge with the the experimental analysis results.

As shown above, research on the determining strain values using the Wheatstone bridge theorem mainly focuses on mass flow measurements in pressure sensors and thin-film composite membranes. There are few studies on

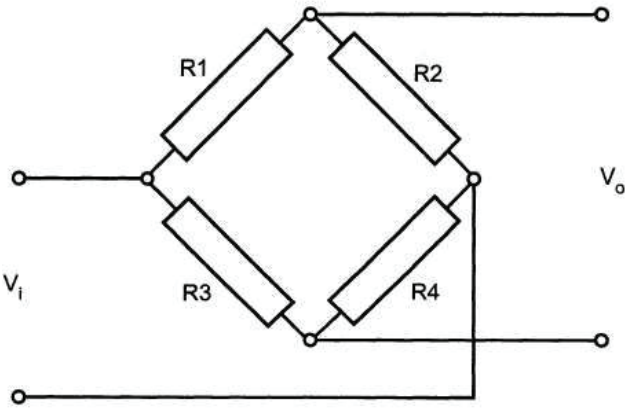

Figure 1. Wheatstone bridge [34].

determining deformation in structural steel under different loading conditions using a Wheatstone bridge theorem.

In this study, the tests for tension, torsion and bending have been performed to investigate using strain gauges under the different mechanical loads. Experimental, theoretical and numerical approaches were used within the study. Geometric models similar to the experimental design were applied to ANSYS finite element program in numerical analyses. Additionally, the strain values were determined theoretically using the full bridge approach in the Wheatstone Bridge Theorem.

Theoretical Approach

In this study, the strain values were determined using the Wheatstone Bridge Theorem (WBT). In WBT, strain measurement was done by resistance changes on the strain gauges. Four identical resistances (R1,R2,R3,R4) take place on the Wheatstone bridge and these resistances are connected end to end in a diamond shape. In addition, voltage calculations have made on identical resistances. An input voltage (V_i) and output voltage (V_0) connects across opposite connection over the Wheatstone bridge. The demonstration of the Wheatstone bridge is given in Figure 1 [34].

In theoretical approach, the strain gauges and their connections should be defined before explaining strain calculation using the Wheatstone bridge.

STRAIN GAUGE

The basic definition of the strain gauge is to measure strains using electrical sensors. In strain calculation, the electrical resistance changes by a small amount when external forces stretches or compress them [34]. This situation provides to determine the strain value. The position of resistance wires on the strain gauge is varied according to the loading conditions. In tension, compression and bending tests, the resistance wires are located on strain gauges with 90 degrees to measure the strain however, in the torsion test, the resistance wires are located on strain gauges with 45 degrees. The strain gauges used in both tension and torsion test are given in Figure 2.

In this study, the strain values were determined using the full bridge connection in the Wheatstone Bridge Theorem.

FULL BRIDGE CONNECTION IN WHEATSTONE BRIDGE THEOREM

In a full bridge connection, strain calculation is done over the four strain gauges located on the bridge. In addition, tensile stress, bending and as well as shear stresses can be calculated by using full bridge connection. The main goal of selecting the full bridge connection is to provide much more voltage output and sensitivity rather than other bridge connections (half bridge and Quarter Bridge). Full bridge strain connections are illustrated in Figure 3.

The calculation of strain values across the full bridge is done according to the standard equation [35];

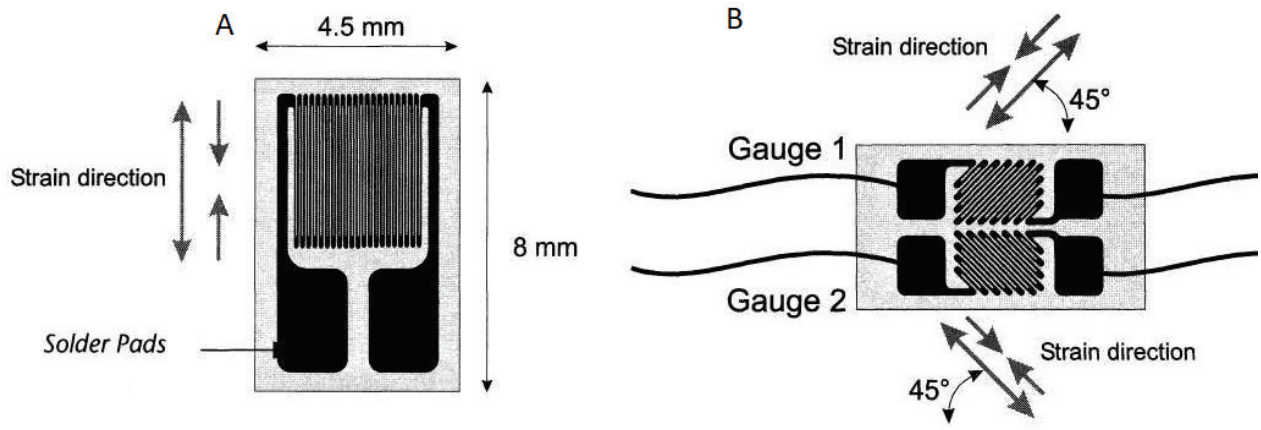

Figure 2. Strain gauges ((A) In tension, compression, bending test, (B) Torsion test) [34].

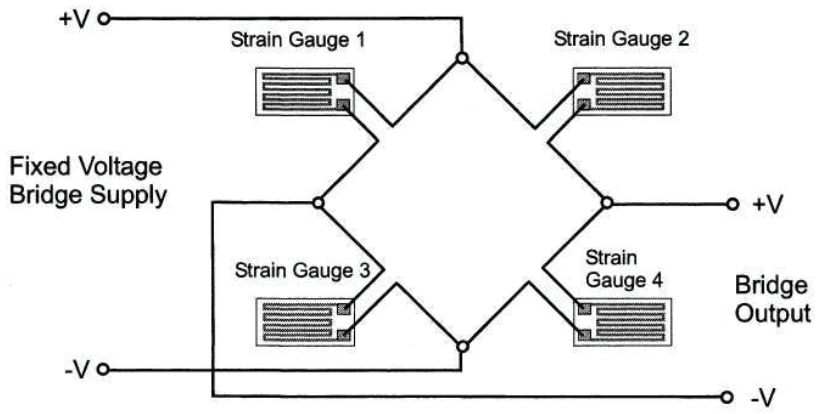

Figure 3. Full bridge connection [34].

$$\varepsilon = 4 \times \frac{V_0}{G_F \times V_i \times N} \tag{1}$$

where, ε is the strain, V_0 is the voltage measured across the bridge, G_F is the gauge factor, V_i is the fixed input voltage and N is the number of active gauges connected.

Determination of Stress Values

In this study, three different stress values were observed. These are bending stress, shear stress and normal stress. When the perpendicular force is applied to the cross-section area of a material, normal stress occurs. The normal stress is shown as below;

$$\sigma = \frac{F}{A} \tag{2}$$

where, σ is the normal stress, F is the force and A is the cross-sectional area. The normal stress is also referred to as tensile or compressive stress depending on the direction of the force.

The bending stress is the normal stress that occurs when an object is subjected to a load which causes it to bend. The formulation of the bending stress is given below;

$$\sigma_B = \frac{M}{I} y \tag{3}$$

where, σ_B is the bending stress, M is the bending moment, y is the vertical distance from the neutral axis and I is the moment of inertia.

The shear stress occurs when the twisting moment is applied to the end of the shaft. This shear stress is determined through the formulation;

$$\tau = \frac{T}{J} c \tag{4}$$

where, τ is the shear stress, T is the torsion, J is the polar moment of inertia and c is the vertical distance from the neutral axis.

Experimental Approach

The strain gauge test system includes tensile, bending and torsion testing devices. In a strain gauge test system, it is possible to see how much strain is applied to different parts under different mechanical stresses. The digital strain displayer could automatically calculate how much voltage and strain are presented and shows the user as a micro-strain. It should be stated here that all experiments were performed in the linear region. The strain gauge test system is depicted in Figure 4.

Three different experiments were carried out using a strain gauge test system. In the bending test, a rectangular section beam was used. The specimen beam was constrained at the one end using a secure clamp. The load was applied to the other end of the beam in the vertical direction (see figure 5). Four standard strain gauges are measured the tensile and compressive strain directly in line with the beam. Two gauges are measured the tensile strain on the top of the beam, and the other two gauges measure the compressive stress underneath the beam [34].

In a tension test, a clamp holds the top of the test specimen. The weight hanger is located at the bottom of the specimen. Two strain gauges are placed on the specimen to measure the strain in two directions on each side of test specimen (see Figure 6).

In the torsion test, the beam has constrained both ends. The one end of the beam is clamped (i.e frictionless support) and the another end is connected to a fixed support. A torque arm provides to twist the beam. Two special torsion strain gauges measure the torsional shear strain on the surface on the beam at 45 degrees to the beam length. The experimental set up is shown in Figure 7. Strain gauges work best when positioned in the direction of the measured strain. The angle between the stress and strain in the bar in the torsion assembly and the longitude of the bar is 45°. Strain is measured using a special rosette consisting of two 45° strain gauges.

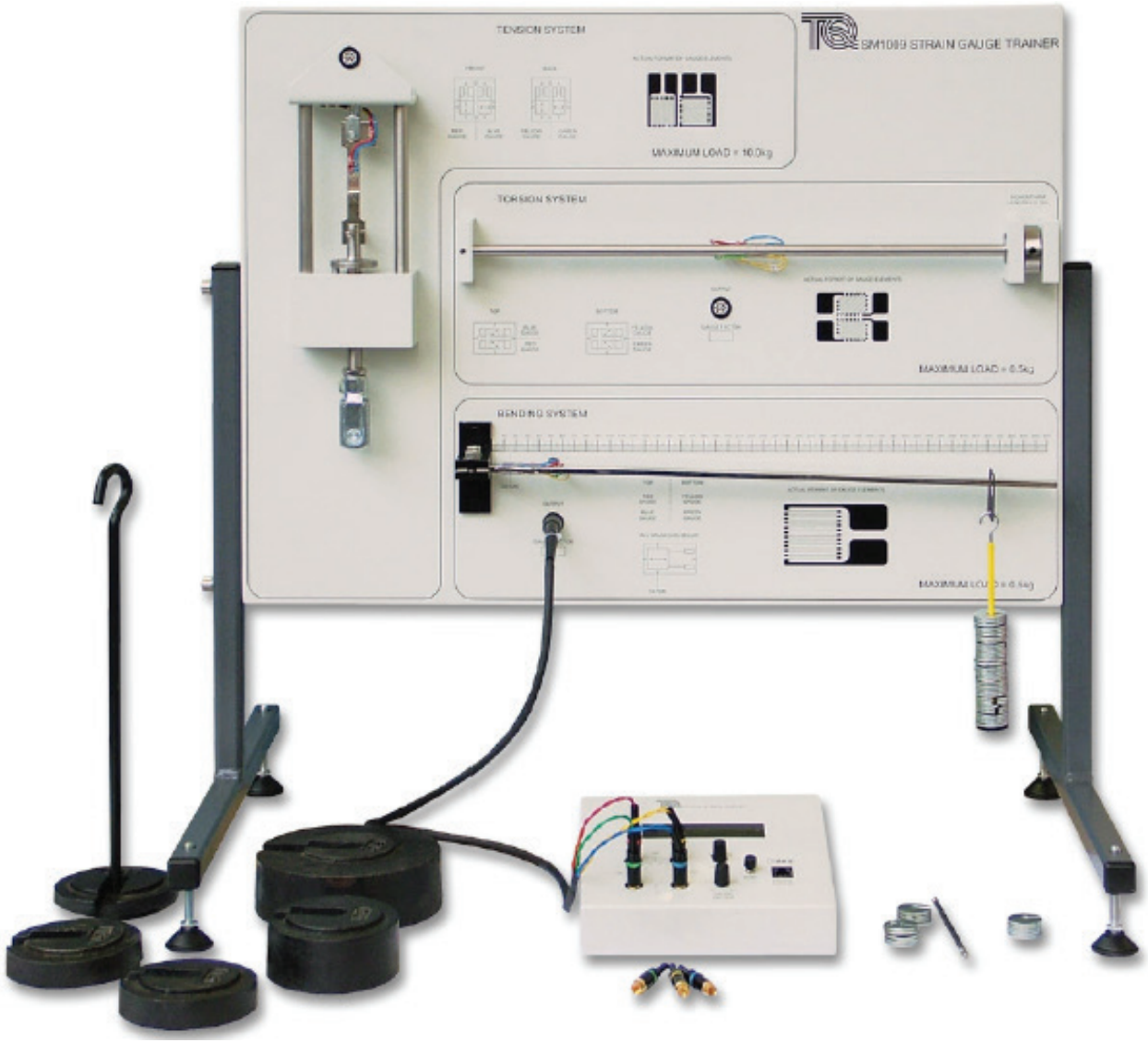

Figure 4. The strain gauge test system.

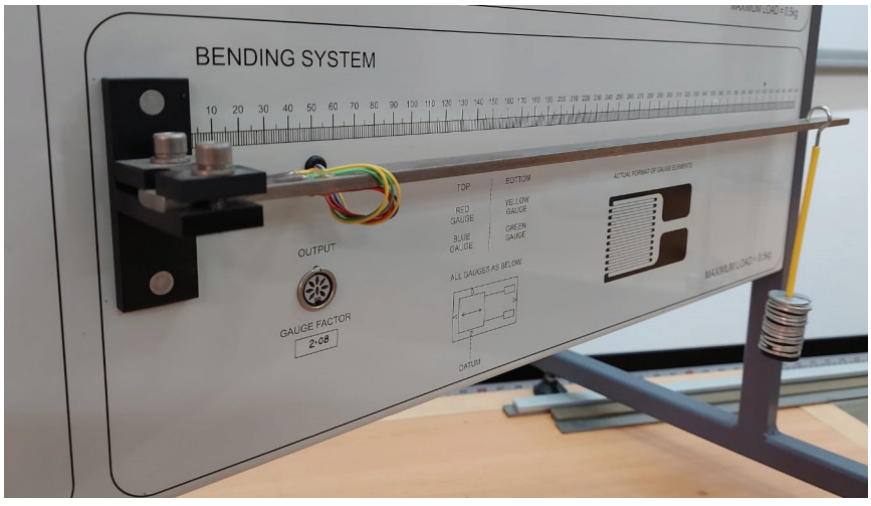

Figure 5. Bending test system.

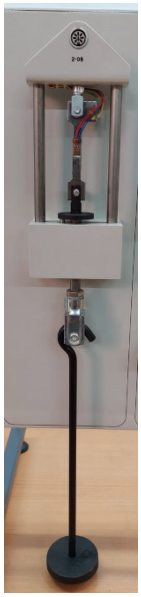

Figure 6. Tensile test system.

Numerical Approach

Numerical analysis was performed using the ANSYS WORKBENCH finite element program. Analyzes were performed in the static-structural analysis module, using solid elements. The numerical model of each tests is created by the experimental conditions. Then, tension, bending and torsion stresses and strains were calculated numerically. In the numerical analysis, firstly, the geometries of the test samples used in each experiment were created in the design CAD program and transferred to the ANSYS finite element program. The boundary conditions used

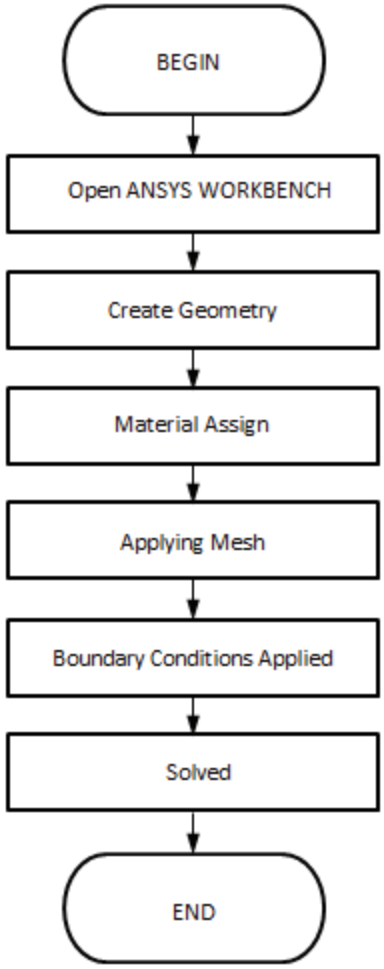

Figure 8. Flowchart of static-structural analysis with ANSYS Workbench.

Figure 7. Torsion test system.

Table 1. Linear-elastic material properties for structural steel

Material	Elastic Modulus (GPa)	Poisson ratio	Yield Strength (MPa)	Shear Modulus (GPa)
Structural Steel	207	0.32	250	79.6

experimental approach was applied to the test specimens in numerical analyses. A parametric study was also implemented to optimize the number and size of the elements. Then, the final mesh for all numerical analyses was consisted of 5000 elements and 12000 nodes approximately. In the numerical model, the linear-elastic behaviour of the material has been studied, evaluating the small deformation. The stiffness behaviour of the elements was arranged as flexible, and the analyzes were carried out in this way. For the modelling of linear-elastic behaviour, it should be entered input data given in Table 1. The data in Table 1 are derived from the properties of the material (Young's

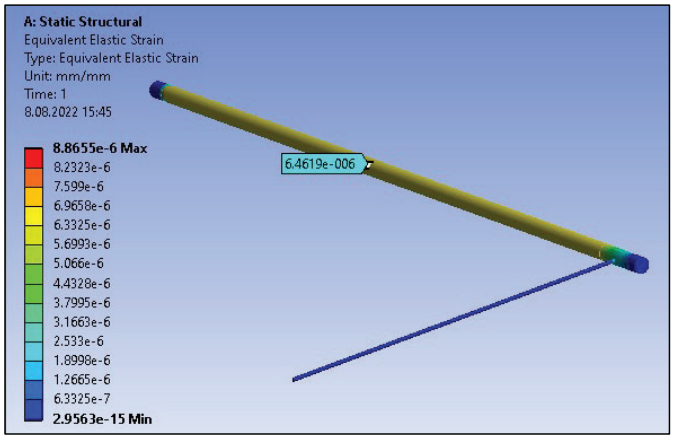

a)

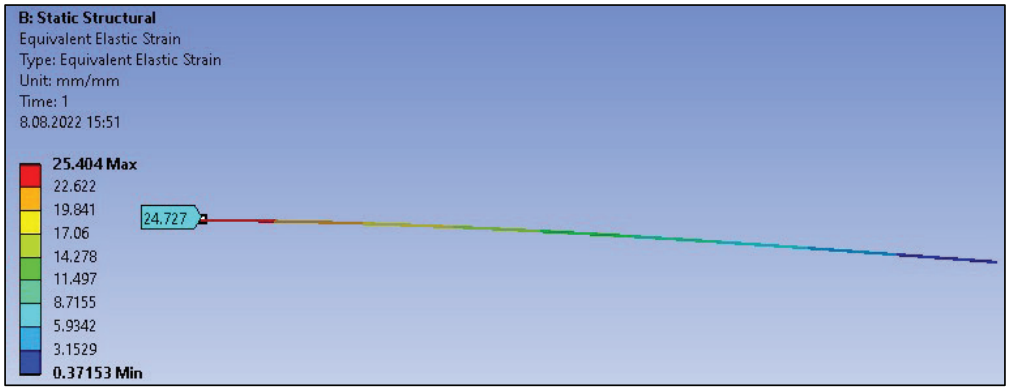

b)

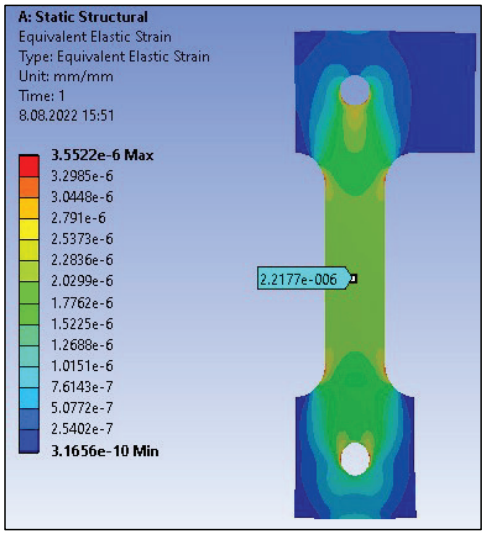

c)

Figure 9. Numerical analyses results ((a) Torsion Test, (b) Bending Test, (c) Tension Test).

modulus, Poisson's ratio, and shear modulus), the evaluated stress, and the strain measured within the elastic range for the applied load. Stress and strain values of the tensile specimen and Young's modulus of the material were found. The material's shear modulus was obtained from shear stress and strain values. Poisson's ratio was found from the relationship between shear modulus and Young's modulus. Then, the data obtained from Table 1 were used in design formulas, and FEA for other loads and strains were found and compared with the measured values.

After the modelling section is completed, the solution is run. In the solution section, equivalent stress and strain values are obtained. The results of numerical analyses are discussed in the relevant sections to facilitate the monitoring of the article. The stages of static-structural analysis with ANSYS Workbench are shown in the flowchart in Figure 8. The reproduction results for each test obtained from the original ANSYS plot are demonstrated in Figure 9.

In the numerical analysis, the mesh has an average element quality of 86%, an aspect ratio of 1.75%, and a skewness ratio of 0.22 in terms of the adequateness of the mesh. In addition, the mesh structure was smoothed using the pinch method, with the tolerance value determined by the element size value for the suitability of the mesh structure. It should also be stated that the element type utilized in finite element analysis is hex dominant.

RESULTS AND DISCUSSION

The aim of this study is to investigate the strain behavior of the steel material under tensile, torsion and bending loads. The strain behaviour was examined through experimental, theoretical and numerical approaches. It is thought that evaluating each test approach separately will facilitate the understanding of the article. Firstly, the results of experimental approaches for each test will be discussed. Secondly, the results of theoretical approach will be given. Thirdly, the results of numerical analyses will be discussed. Finally, the results of all approaches will be compared to each other.

In bending tests, consecutive loads were applied to the rectangular cross-section beam. The dimensions of the beam (19.32 mm x 4.83 mm x 500 mm) were used in the experiment. The strain values were noted during the experiments using a digital strain displayer. The bending stresses were determined by the test device interface program (VDAS). The stress and strain values of steel material under bending loads are given in Table 2.

After obtaining the experimental results, the theoretical approach was carried out. In the theoretical approach, the strain values were calculated using Equation 1, and the bending stresses were calculated using Equation 3. In strain calculation, the gauge factor and input voltage value were used 2.04 and 5.3 μV respectively. It should be stated here that the gauge factor varies slightly between 1.9-2.3 for metallic materials.

The data used in the theoretical calculations are given in Table 3.

In addition, the moment of inertia of the beam is used as $1.8x10^{-10}$ m^4 in stress calculation. Eventually, the numerical analyses were carried out by accordance with the experimental and theoretical approaches. All results are demonstrated in Figure 10.

Table 2. Bending stress and strain values of steel material

Load (N)	Stress (MPa)	Strain (με)
0.98	5.29	26
1.96	10.58	51
2.94	15.87	77
3.92	21.16	102
4.91	26.45	128

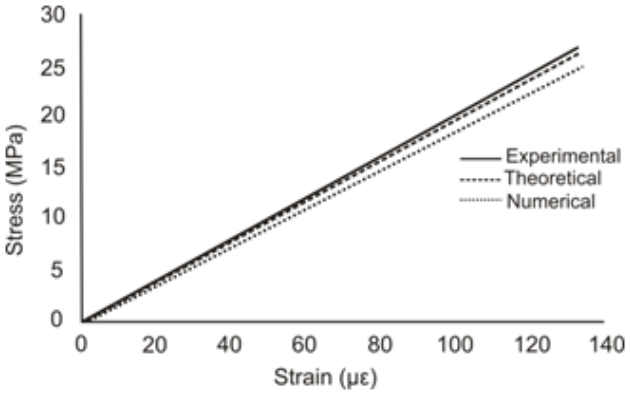

Figure 10. Stress-Strain values for bending.

Table 3. The data used in the theoretical calculations in bending

Load (N)	Output voltage (μV)	Bending Moment (Nm)	Strain (με)
0.98	277	0.397	24
1.96	555	0.795	53
2.94	834	1.192	79
3.92	1112	1.589	100
4.91	1393	1.986	129

Table 4. Shear stress and strain values of steel material

Load (N)	Stress (MPa)	Strain (με)
1.227	0.945	6
2.4525	1.89	12
3.6725	2.835	18
4.9050	3.78	24

In torsion tests, consecutive loads were applied to the circular beam. The beam used in the torsion tests has a length of 486 mm and a diameter of 9.86 mm. In experiments, the strain values were noted using a digital strain displayer. The torsion stresses were determined by VDAS. The stress and strain values of steel material under torsion loads were given in Table 4.

In the theoretical approach, the strain values were calculated using Equation 1 and the shear stresses were calculated using Equation 4. In strain calculation, the gauge factor and input voltage value were used 2.04 and 10.62 μV respectively. The data used in the theoretical calculations are given in Table 5.

The polar moment of inertia of the beam is used as $9.7x10^{-10}$ m^4 in stress calculation. Finally, the numerical analyses were implemented, and stress-strain values were obtained. All results are shown in Figure 11.

Table 5. The data used in the theoretical calculations in torsion

Load (N)	Output voltage (μV)	Torque (Nm)	Strain (με)
1.227	65	0.183	7
2.4525	130	0.367	12
3.6725	195	0.552	19
4.9050	260	0.736	24

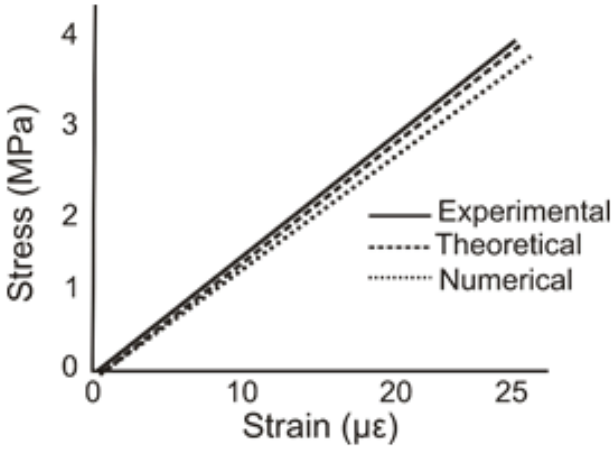

Figure 11. Stress-Strain values for torsion.

In tension tests, consecutive loads were applied to the dog-bone specimen. The dimensions of dog-bone specimen are 10.06 mm x 2.02 mm x 77 mm. The cross-section area of the tensile specimen is $203x10^{-7}m^2$. In experiments, the strain values were noted using a digital strain displayer, and the normal stresses were determined by VDAS. The stress and strain values of steel material under tension loads were given in Table 6.

In the theoretical approach, the strain values were calculated using Equation 1 and the normal stresses were calculated using Equation 2. In strain calculation, the gauge factor and input voltage value were used 2.04 and 22.05 μV respectively. The data used in the theoretical calculations are given in Table 7.

Consequently, numerical analyses of the tension test was completed, and the results were compared. All results are given in Figure 12.

Table 6. Normal stress and strain values of steel material

Load (N)	Stress (MPa)	Strain (με)
9.81	0.48	2
19.62	0.97	4
29.43	1.45	6
39.24	1.93	8
49.05	2.42	11
58.86	2.90	13
68.67	3.38	15
78.48	3.87	17
88.29	4.35	20
98.1	4.83	22

Table 7. The data used in the theoretical calculations in tension

Load (N)	Output voltage (μV)	Strain (με)
9.81	45	2
19.62	90	5
29.43	135	7
39.24	180	9
49.05	225	12
58.86	270	14
68.67	315	15
78.48	360	18
88.29	405	20
98.1	450	23

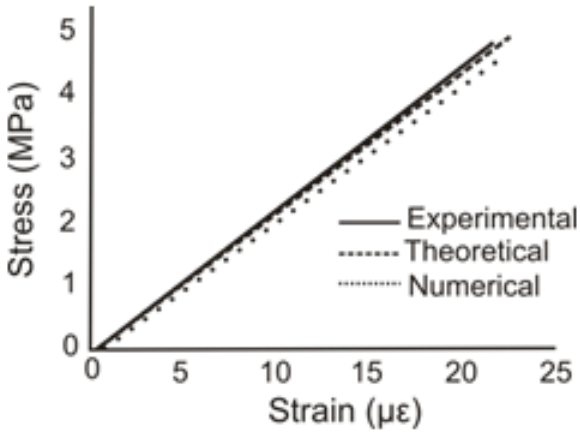

Figure 12. Stress-Strain values for tension.

When the results were evaluated, it was concluded that the use of strain gauges was appropriate for experimental, theoretical and numerical approaches to each tests.

CONCLUSION

In this study, tension, torsion and bending tests were performed in order to determine the strain values of the steel material. Besides the experimental tests, numerical and theoretical approaches were implemented to ensure the test results. The strain values were determined theoretically using the full bridge approach in Wheatstone Bridge Theorem. Numerical analysis was implemented using ANSYS finite element program. This study is not intended to determine the strain changes occurring in the nonlinear region in all approaches. Because the main goal of this study is to determine the suitability of using strain gauge for bending, torsion and tension experiments. From the results of the experimental tests with the test stand SM 1009 and the numerical analysis using the ANSYS finite element program, we can draw the following conclusions:

1. A deformation on structural steel was found using a Wheatstone bridge, the study helps to find the properties of a new material and also to understand the material deformation of complex configurations through finite element analysis, stress and strain distributions under different loading conditions (Torsion, tension and bending) can be determined.
2. It was compared to the strain values. As a result, for the tensile, bending, and torsion tests, the mean error values between theoretical and numerical are, respectively, 5.17%, 4.23%, and 6.26%. The same tests had mean error values of 7.08%, 3.48%, and 4.89% between the theoretical and experimental findings, respectively.
3. At the end of the studies, it was seen that the results obtained from all approaches indicated similar tendencies with each other. Therefore, it can be interpreted that using the use of the strain gauge in bending, torsion and tensile tests is quite appropriate.
4. Determination of strain values using the Wheatstone Bridge Theorem takes in the limited study in the existing literature. Therefore, it is expected that this study can make a contribution to the existing literature.

The deformation and stress values for different loadings on the structural steel were determined by experimental, theoretical, and finite element approaches utilizing a Wheatstone bridge. It was observed that the results converged with each other. However, the determination of the deformation and stress values of the steel material, which is widely used with Wheatstone bridge for different loading conditions, is thought to make an essential contribution to the literature since it has not been studied before.

AUTHORSHIP CONTRIBUTIONS

Authors equally contributed to this work.

DATA AVAILABILITY STATEMENT

The authors confirm that the data that supports the findings of this study are available within the article. Raw data that support the finding of this study are available from the corresponding author, upon reasonable request.

CONFLICT OF INTEREST

The author declared no potential conflicts of interest with respect to the research, authorship, and/or publication of this article.

ETHICS

There are no ethical issues with the publication of this manuscript.

REFERENCES

[1] Theo F, Dietrich M, Gerhard T. Nonsymmetric deformation behavior of lead zirconate titanate determined in bending tests. J Am Ceram Soc 1998;81:269–272. [CrossRef]

[2] Talesnick ML, Ringel M. Completing the hollow cylinder methodology for testing of transversely isotropic rocks: torsion testing. Int J Rock Mech Min Sci 1999;36:627–639. [CrossRef]

[3] Theo F, Dietrich M, Gerhard T. Multiaxial deformation behavior of PZT from torsion tests. J Am Ceram Soc 2003;86:1427–1429. [CrossRef]

[4] Daniel G, Gerrit D, Walter L. Simultaneous measurement of strain and temperature with two resistive strain gauges made from different materials. Procedia Manuf 2018;24:258–263. [CrossRef]

[5] Ignakhin VS, Severikov VS, Grishin AM. Tensile and torsional strain gauge based on Fe48Co32P14B6 metallic glass. J Magn Magn Mater 2019;476:382–386. [CrossRef]

[6] Çetin M, Turan ME, Aydın F, Sun Y. Residual stress measurement by strain gauge and X-ray diffraction method in different shaped rails. Eng Fail Anal 2019;96:525–529. [CrossRef]
[7] Edwards JR, Gao Z, Wolf HE, Dersch M, Qian Y. Quantification of concrete railway sleeper bending moments using surface strain gauges. Measurement 2017;111:197–207. [CrossRef]
[8] Bazán AM, Gálvez JC, Reyes E, Galé-Lamuela D. Study of the rust penetration and circumferential stresses in reinforced concrete at early stages of an accelerated corrosion test by means of combined SEM, EDS and strain gauges. Constr Build Mater 2018;184:655–667. [CrossRef]
[9] Tavakolpour-Saleh AR, Setoodeh AR, Gholamzadeh M. A novel multi-component strain-gauge external balance for wind tunnel tests: Simulation and experiment. Sens Actuators A Phys 2016;247:172–186. [CrossRef]
[10] Zhou K, Wu ZY. Strain gauge placement optimization for structural performance assessment. Eng Struct 2017;141:184–197. [CrossRef]
[11] Cozzolino F, Apicella D, Wang G, Apicella A, Sorrentino R. Implant-to-bone force transmission: A pilot study for in vivo strain gauge measurement technique. J Mech Behav Biomed Mater 2019;90:173–181. [CrossRef]
[12] Ferrero C. Thermal and magnetic correlation in apparent strain down to 1.53 K and up to 6 T on strain gauges. Measurement 2018;128:403–409. [CrossRef]
[13] Walstrom PL. Strain gauges for superconducting magnet testing. Cryogenics 1980;20:509–512. [CrossRef]
[14] Soto AG, Caldentey AP, Peiretti HC, Benitez JC. Experimental behaviour of steel-concrete composite box girders subject bending, shear and torsion. Eng Struct 2020;206:110169. [CrossRef]
[15] Iriarte X, Aginaga J, Gainza G, Ros J, Bacaicoa J. Optimal strain-gauge placement for mechanical load estimation in circular cross-section shafts. Measurement 2021;174:108938. [CrossRef]
[16] Zeinali E, Nazari A, Showkati H. Experimental-numerical study on lateral-torsional buckling of PFRP beams under pure bending. Compos Struct 2021;237:111925. [CrossRef]
[17] Wan HX, Huang B, Mahendran M. Experiments and numerical modelling of cold-formed steel beams under bending and torsion. Thin Wall Struct 2021;161:107424. [CrossRef]
[18] Chang Y, Wen W, Xu Y, Cui H, Xu Y. Quasi-static mechanical behavior of filament wound composite thin-walled tubes: Tension, torsion, and multi-axial loading. Thin-Wall Struct 2022;177:109361. [CrossRef]
[19] Sadeghi MZ, Weiland J, Zimmermann J, Schiebahn A, Reisgen U, Schröder KU. Experimental and FE investigations on the influential parameters in positioning and measurement of strain gauges in adhesively bonded single lap joints. Procedia Struct Integr 2020;28:1590–1600. [CrossRef]
[20] Casiraghi C, Macucci M, Parvez K, Worsley R, Shin Y, Bronte F, et al. Inkjet printed 2D-crystal based strain gauges on paper. Carbon 2018;129:462–467. [CrossRef]
[21] Ren S, Jiang S, Liu H, Zhang W, Li Y. Investigation of strain gauges based on interdigitated Ba0.5Sr0.5TiO3 thin film capacitors. Sens Actuators A Phys 2015;236:159–163. [CrossRef]
[22] Enser H, Kulha P, Sell JK, Jakoby B, Hilber W, Straub B, et al. Printed strain gauges embedded in organic coatings. Procedia Eng 2016;168:822–825. [CrossRef]
[23] Popplewell H, Carré M, Lewis R. Measurement of finger pad forces and friction using finger nail mounted strain gauges. Wear 2017;376:295–304. [CrossRef]
[24] Guo Z, Xu J, Chen Y, Guo Z, Yu P, Liu Y, et al. High-sensitive and stretchable resistive strain gauges: Parametric design and DIW fabrication. Compos Struct 2019;223:110955. [CrossRef]
[25] Chadha M, Todd MD. A comprehensive kinematic model of single-manifold Cosserat beam structures with application to a finite strain measurement model for strain gauges. Int J Solids Struct 2019;159:58–76. [CrossRef]
[26] Castro HF, Correia V, Pereira N, Costab P, Oliveiraa J, Lanceros-Méndez S. Printed Wheatstone bridge with embedded polymer based piezoresistive sensors for strain sensing applications. Addit Manuf 2018;20:119–125. [CrossRef]
[27] Al-Badry LF. Possibility of designing molecular Wheatstone bridge: Electrostatic and conformational. Solid State Commun 2021;331:114297. [CrossRef]
[28] Tan X, Lv Y, Zhou X, Song X, Wang Y, Gu G, et al. High performance AlGaN/GaN pressure sensor with a Wheatstone bridge circuit. Microelectron Eng 2020;219:111143. [CrossRef]
[29] Ang WC, Kropelnicki P, Tsai JML, Leong KC, Tan CS. Design, simulation and characterization of Wheatstone Bridge structured metal film uncooled microbolometer. Procedia Eng 2014;94:6–13. [CrossRef]
[30] Gotszalk T, Grabiec P, Rangelow IW. Calibration and examination of piezoresistive Wheatstone bridge cantilevers for scanning probe microscopy. Ultramicroscopy 2003;97:385–389. [CrossRef]
[31] Karode SK, Kulkarni SS. Analysis of transport through thin film composite membranes using an improved Wheatstone bridge resistance model. J Membrane Sci 1997;127:131–140. [CrossRef]
[32] Rozumek D, Marciniak Z. Control system of the fatigue stand for material tests under combined bending with torsion loading and experimental results. Mechanical Systems and Signal Processing. 2008;22:1289–1296. [CrossRef]
[33] Svete A, Kutin J, Bajsić I. Static and dynamic characteristics of a hydraulic Wheatstone bridge mass flowmeter. Flow Meas Instrum 2009;20.6:264–270. [CrossRef]

[34] TecQuipment. SM1009 Strain gauge trainer user guide. Available at: https://www.studocu.com/row/document/bilkent-universitesi/fundamentals-of-mechanical-engineering/sm-1009-strain-gauge-trainer-user-guide/36476430. Accessed on May 15, 2024.

[35] Karl H. Applying the wheatstone bridge circuit. Available at: http://eln.teilam.gr/sites/default/files/Wheatstone%20bridge.pdf. Accessed on May 14, 2024.